Supplementary Information

Visible-light-driven oxygen evolution by $BaTiO_3$ based ferroelectric photocatalyst via water splitting

Areef Billah*, Anjuman Nesa Anju, Fumihiko Hirose, and Bashir Ahmmad†
Graduate School of Science and Engineering, Yamagata University,
4-3-16 Jonan, Yonezawa, Yamagata 992-8510, Japan

*Corresponding author: areefbillah@gmail.com
†Corresponding author: arima@yz.yamagata-u.ac.jp

Supplementary Table 1: Rietveld refinements were performed for all the prepared materials. Quantified parameters such as space group, lattice constants, volume, density, goodness of fitting (χ^2), Bragg R-factor, and RF-factor are summarized in the following table.

Sample	Space group	Lattice Constant		Volume	Density (g/cm^3)	χ^2	Bragg R-factor	RF-factor
		a	c					
MN-0	P4mm	3.9993	4.0357	64.5504	5.999	1.37	3	1.85
MN-2.5	P4mm	4.00303	4.03112	64.5935	6.06	1.53	4.659	2.791
MN-5	P4mm	4.00565	4.02848	64.7146	6.018	1.46	4.569	3.049
MN-7.5	P4mm	4.01038	4.02334	65.5934	5.953	1.5	2.302	1.329
MN-10	Pm-3m	4.0153	4.0153	64.7369	6.049	1.39	3.078	2.028

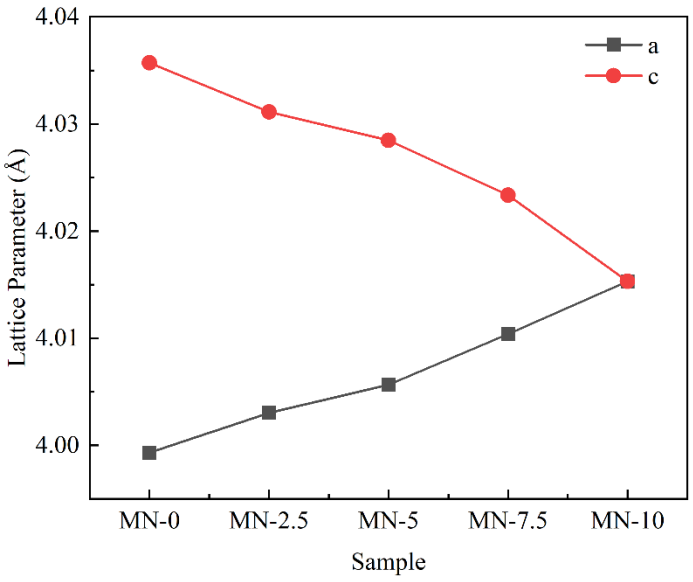

Supplementary Figure S1: Lattice constants of undoped and doped $BaTiO_3$ as a function of doping concentration.

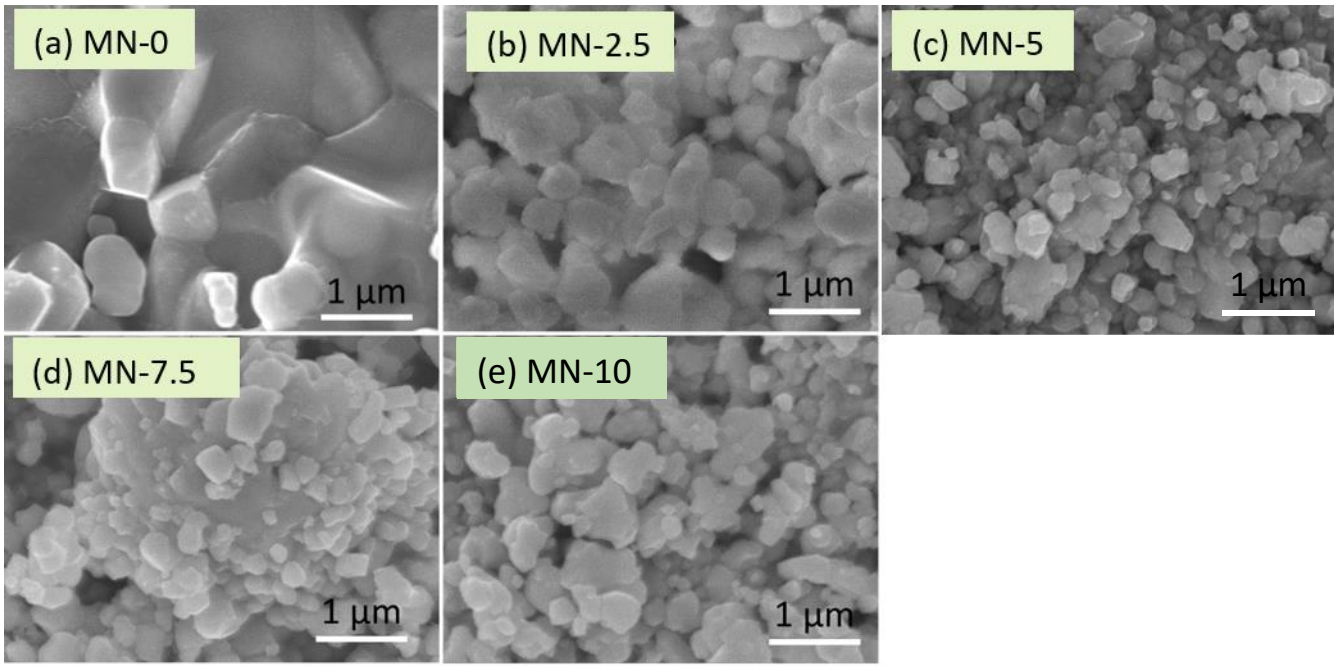

Supplementary Figure S2: Field Emission Electron Microscopy (FE-SEM) images of (a) MN-0, (b) MN-2.5, (c) MN-5, (d) MN-7.5 and (e) MN-10.

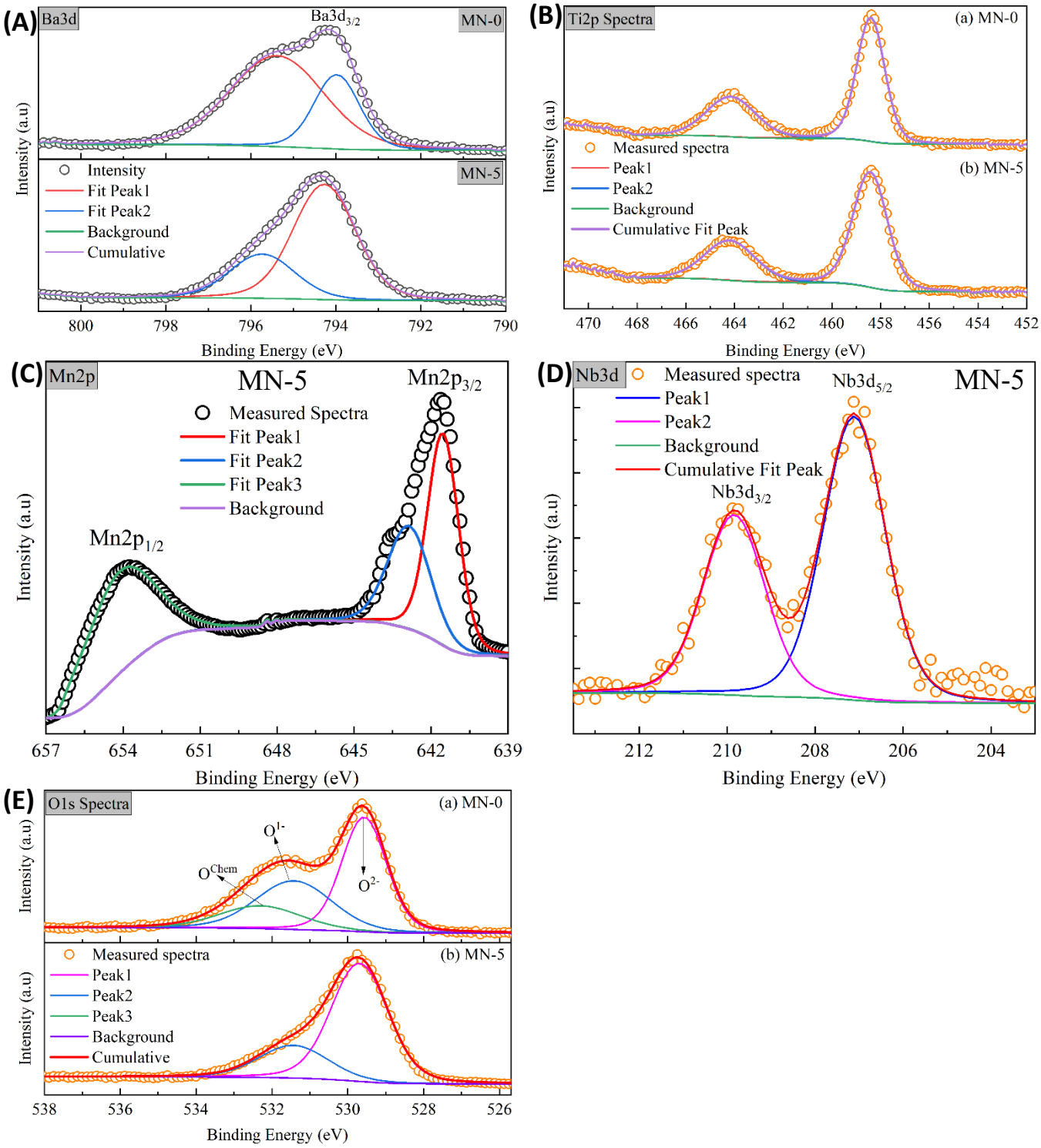

Supplementary Figure S3: X-ray photoelectron spectroscopy (XPS) spectra of (A) Ba3d, (B) Ti2p, (C) Mn2p, (D) Nb3d, and (E) O1s orbitals. The deconvoluted components of measured peaks are obtained by Gaussian fitting with Shirley-type background using CasaXPS software.

XPS analysis: The spectra for Ba3d, Ti2p, Mn2p, Nb3d and O1s orbitals were measured with a dedicated scan, and the obtained data were deconvoluted with Gaussian fitting having Shirley type background using

CasaXPS software. For the MN-0 sample, the peak observed at 794.12 eV represents Ba3d orbital, where it can be resolved into two components such as at 793.99 eV and 795.39 eV. Similarly, the two components are located at 794.26 eV and 795.74 eV with different areas for MN-5 materials. The Ti2p peak is separated into two parts, $Ti2p_{3/2}$ and $Ti2p_{1/2}$, which are positioned at approximately 458.44 eV and 464.26 eV, respectively, for both MN-0 and MN-5 materials. The binding energies of Ti2p peaks corroborate its chemical bonding with oxygen ions [1]. The orbital spectra of Mn2p (dopant element) have two peaks $Mn2p_{3/2}$ and $Mn2p_{1/2}$, which are located at 641.54 eV and 653.80, respectively. However, $Mn2p_{3/2}$ can be deconvoluted into two components at 641.54 eV and 642.91 eV. Another doping content is Nb and its spectra for Nb3d orbital was observed at 209.83 eV ($Nb3d_{3/2}$) and 207.12 ($Nb3d_{5/2}$). Both the Mn2p and Nb3d orbital spectra confirm the presence of dopant ions within the material and their chemical bonding with oxygen atom [2,3]. Fig. S2 shows wide and asymmetric peaks for both the MN-0 and MN-5 samples, which gives a clear hint that there are additional chemical states of oxygen [4]. Gaussian fitting for the undoped sample reveals that it has three components, where the first peak at 529.56 is attributed to the divalent O^{2-} anions, the second peak at 531.44 eV represents monovalent O^{1-} anions, and the last peak at a relatively higher binding energy of 532.32 eV is assumed to be chemically absorbed oxygen [5]. On the other hand, the MN-5 sample shows two components for divalent and monovalent anions at 529.68 eV and 531.48 eV, respectively.

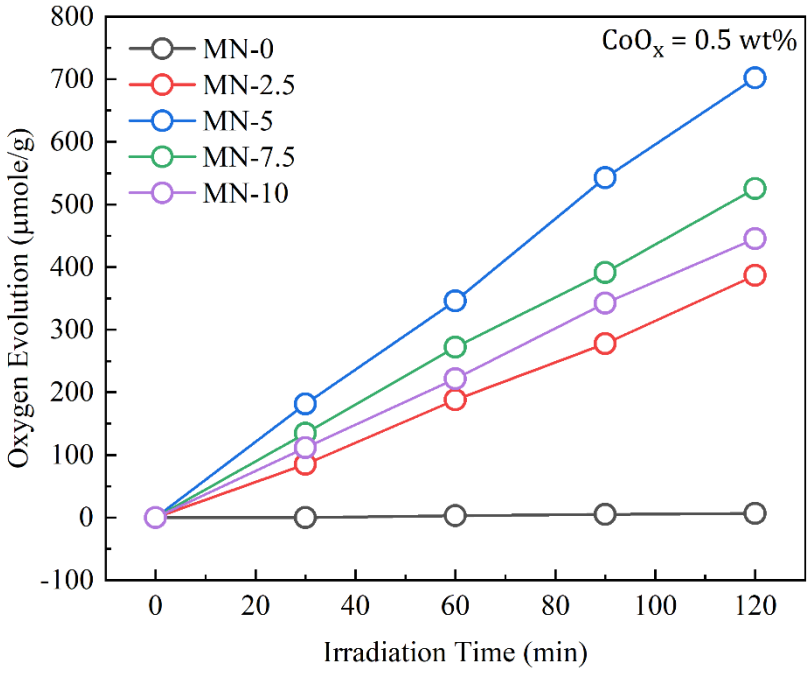

Supplementary Figure S4: Photocatalytic oxygen evolution through water-splitting under visible light exposure. Each photocatalyst used in this experiment is modified by 0.5 wt% CoO_x cocatalyst.

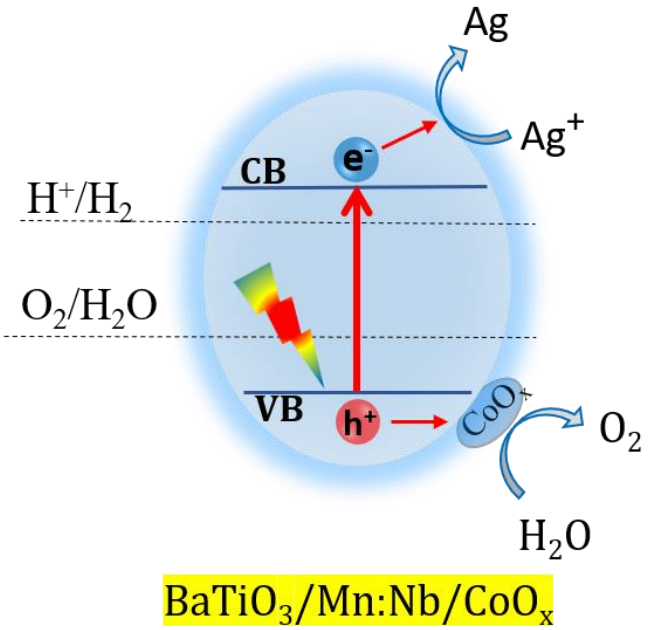

Supplementary Figure S5: The probable mechanism for oxygen evolution. Photogenerated holes of the photocatalyst reacts with water to produce O_2. CoO_x co-catalysts promote the separation of photogenerated charge carriers and increase catalytically active sites [6]. On the other hand, photogenerated electrons are consumed by the sacrificial agents (AgNO3) in the reaction solution [7].

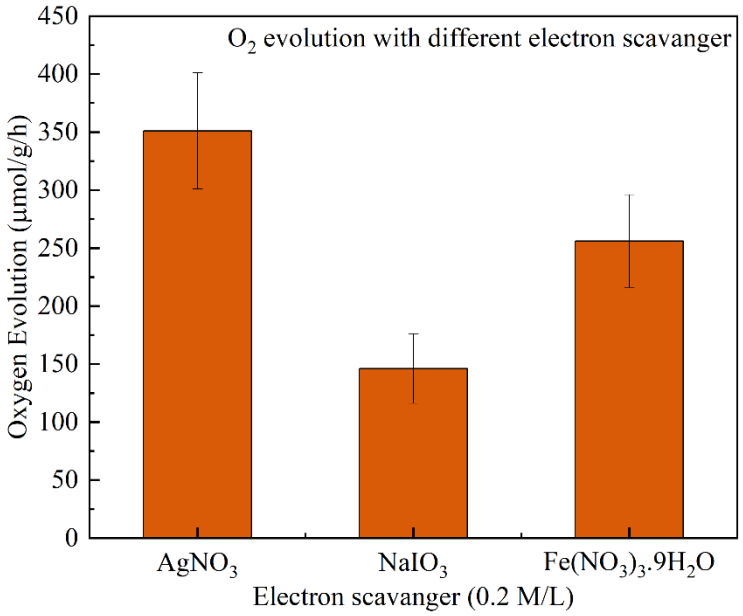

Supplementary Figure S6: Oxygen evolution with different electron scavenger for 0.5 wt% CoO_x deposited MN-5 sample.

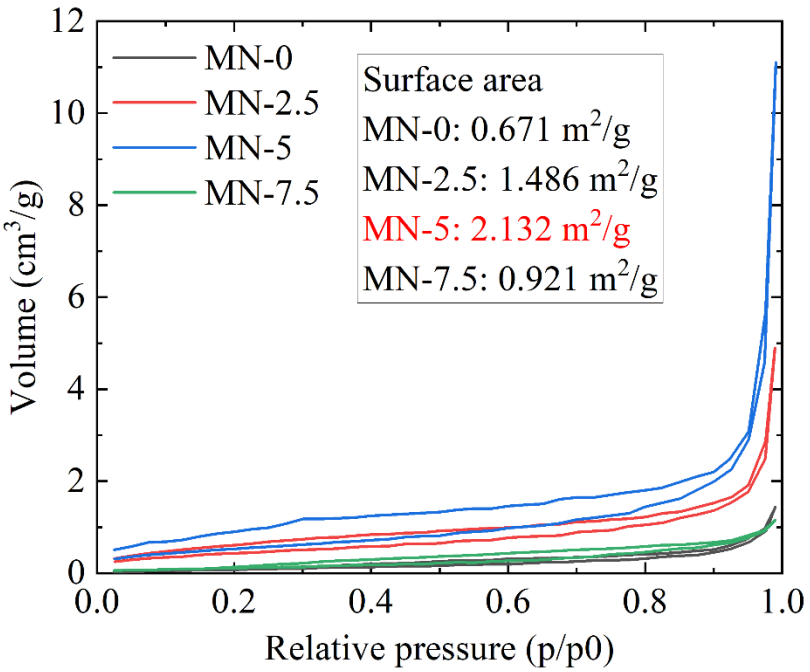

Supplementary Figure S7: Nitrogen adsorption-desorption isotherm and specific surface area for the synthesized materials.

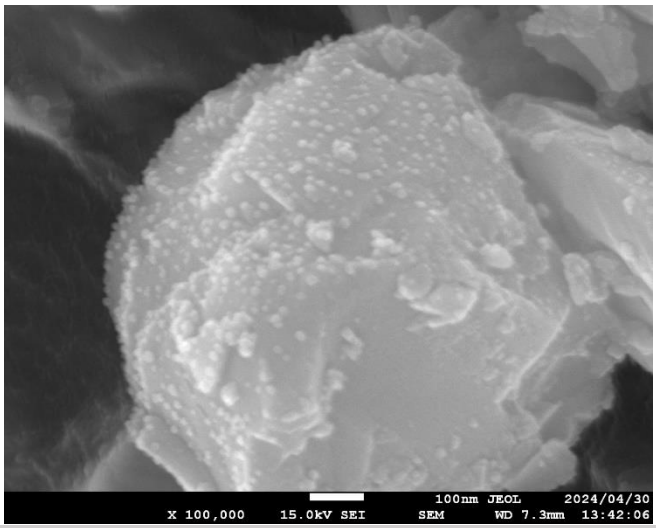

MN-5/CoO_x: Before Oxygen Evolution

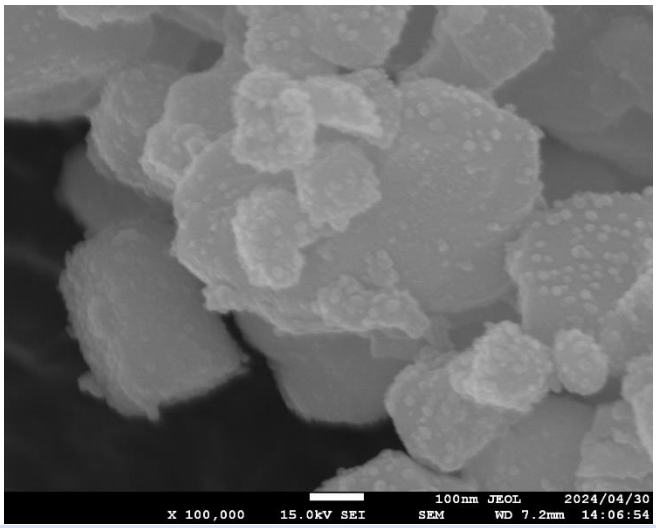

MN-5/CoO_x: After Oxygen Evolution

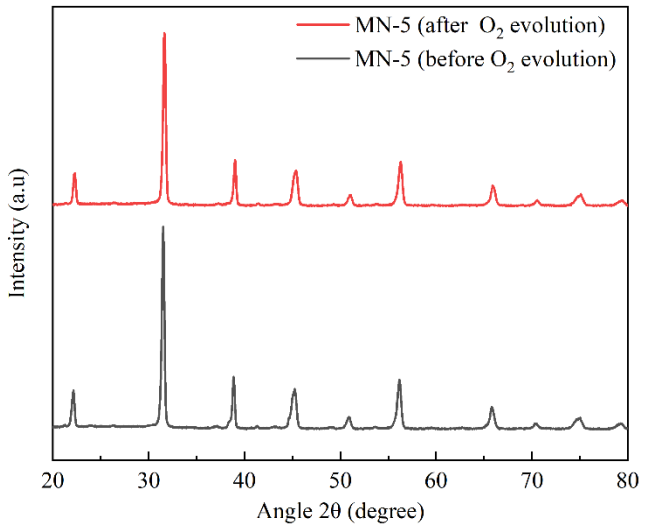

XRD spectra

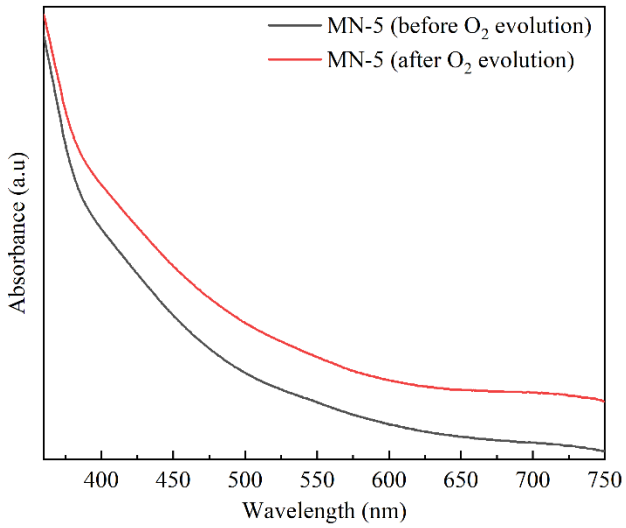

Absorbance spectra

Supplementary Figure S8: FE-SEM images, XRD patterns and Absorbance spectra of CoO_x deposited MN-5 sample before and after oxygen evolution.

Reference:

1. M.C. Biesinger, L.W.M. Lau, A. Gerson, R.St.C. Smart, *Appl. Surf. Sci.*, 2010, **257**, 887-898.
2. M.C. Biesinger, B.P. Payne, A.P. Grosvenor, L.W.M. Lau, A.R. Gerson, R.St.C. Smart, *Appl. Surf. Sci.*, 2011, **257**, 2717.
3. V.I. Chukwuike, K. Rajalakshmi, R.C. Barik, *Appl. Surf. Sci.*, 2021, **4**, 100079.
4. A. Billah, I. Hossain, A. Nahar, M. Hasan, M. K. Roly, A. N. Anju, K. Saito, F. Hirose, B. Ahmmad and S. M. Hoque, *J. Magn. Magn. Mater.*, 2023, **565**, 170302.
5. L.Q. Wu, S.Q. Li, Y.C. Li, Z.Z. Li, G.D. Tang, W.H. Qi, L.C. Xue, L.L. Ding and X.S. Ge, *Appl. Phys. Lett.*, 2016, **108**, 021905.
6. T. Wu, P. Niu, Y. Yang, L-C. Yin, J. Tan, H. Zhu, J. T. S. Irvine, L. Wang, G. Liu, and H-M. Cheng, *Adv. Funct. Mater.,* 2019, **29**, 1901943.
7. Z. Shen, Y. Zhang, G. Zhang, and S. Liu, *Molecules*, 2023, **28**, 7500.